NANOSYSTEMS:
PHYSICS, CHEMISTRY, MATHEMATICS

Original article

Kolmanovich D.D., et al. *Nanosystems: Phys. Chem. Math.*, 2024, **15** (3), 352–360.
http://nanojournal.ifmo.ru
DOI 10.17586/2220-8054-2024-15-3-352-360

Cellular uptake of FITC-labeled $Ce_{0.8}Gd_{0.2}O_{2-x}$ nanoparticles in 2D and 3D mesenchymal stem cell systems

Danil D. Kolmanovich[1,a], Nikita N. Chukavin[1,2,b], Nikita A. Pivovarov[1,c], Sergey A. Khaustov[2,d], Vladimir K. Ivanov[3,e], Anton L. Popov[1,2,f]

[1]Institute of Theoretical and Experimental Biophysics of the Russian Academy of Sciences, Pushchino, Russia
[2]Scientific and Educational Center, State University of Education, Moscow, Russia
[3]Kurnakov Institute of General and Inorganic Chemistry of the Russian Academy of Sciences, Moscow, Russia

[a]kdd100996@mail.ru, [b]chukavinnik@gmail.com, [c]nikitapivovarov.workmail@gmail.com,
[d]sergeykhaustov@gmail.com, [e]van@igic.ras.ru, [f]antonpopovleonid@gmail.com

Corresponding author: Anton L. Popov, antonpopovleonid@gmail.com

ABSTRACT Cerium-containing nanoparticles have recently been identified as promising nanozymes for advanced biomedical applications. Additional modification of the core or the surface of CeO_2 nanoparticles (CeO_2 NPs) provides them with new functionalities, making them a unique theranostic agent. In this study, dextran-stabilized CeO_2 NPs doped with Gd ($Ce_{0.8}Gd_{0.2}O_{2-x}$) were synthesized and further functionalized with fluorescein isothiocyanate (FITC). The synthesized nanoparticles have a high degree of biocompatibility at concentrations up to 5 mg/mL and are readily internalized by human mesenchymal stem cells cultured both in monolayers (2D system) and cellular spheroids (3D system). The functionalization of CeO_2 NPs with Gd and FITC dye allows for monitoring their accumulation within organs and tissues using both magnetic resonance imaging (MRI) and fluorescence spectroscopy techniques.

KEYWORDS nanoparticles, 3D cell spheroid, cerium, gadolinium

ACKNOWLEDGEMENTS The work was supported by the Russian Science Foundation (project No. 22-73-10231, https://rscf.ru/project/22-73-10231/

FOR CITATION Kolmanovich D.D., Chukavin N.N., Pivovarov N.A., Khaustov S.A., Ivanov V.K., Popov A.L. Cellular uptake of FITC-labeled $Ce_{0.8}Gd_{0.2}O_{2-x}$ nanoparticles in 2D and 3D mesenchymal stem cell systems. *Nanosystems: Phys. Chem. Math.*, 2024, **15** (3), 352–360.

1. Introduction

Currently, cerium dioxide is considered one of the most promising biomedical nanomaterials (CeO_2 NPs) [1–5]. CeO_2 nanoparticles show pronounced antioxidant activity, which allows to suppress the intracellular oxidative stress and inflammation [6]. The antioxidant property of CeO_2 NPs is based on their ability to mimic the activity of various endogenous enzymes, such as SOD [7], catalase [8, 9], phosphatase [10], DNAse [11], phospholipoperoxidase [12] and others [13]. It is generally accepted that this process is based on the redox cycling of Ce^{3+} and Ce^{4+}, and it is attributed to the rapid self-repairing cycle of Ce^{3+}/Ce^{4+} after the inactivation of reactive oxygen species (ROS) [14–18]. Interestingly, the enzyme-like activity of CeO_2 NPs can be modulated by adjusting the size, shape, core composition and surface stabilizer of the particles [19–21]. The use of various biocompatible stabilizers and surfactants not only ensures increased colloidal stability, but also enhances the efficiency of nanoparticle endocytosis and, consequently, provides them with selective cytotoxicity [22]. It has previously been demonstrated that CeO_2 NPs can be internalized by various cell types, such as mesenchymal stem cells [23]. At the same time, the uptake process of CeO_2 NPs by human MSCs is quite complex, as this type of cells does not have a specific function for phagocytosis [24]. In particular, it has been shown that CeO_2 NPs are able to stimulate the proliferation of mouse embryonic fibroblasts [25] and human MSCs, isolated from human tooth pulp [26, 27] and human Wharton's jelly [28]. Surface modification of polymer scaffolds with CeO_2 NPs enhances stem cell proliferation and osteogenesis. Particularly, it has been shown earlier that porous polylactic acid (PLA) scaffolds prepared by 3D printing and decorated with CeO_2 NPs enhanced human mesenchymal stem cell growth, reduced oxidative stress levels in the cells and showed enhanced antibacterial activity against both Gram-negative and Gram-positive bacterial strains [29]. CeO_2 NPs-functionalized poly(ε-caprolactone) (PCL)-gelatin electrospun fibers showed superoxide dismutase (SOD)-mimetic activity and enhanced fibroblast proliferation up to ~ 48 % in comparison to the control [30]. Human umbilical cord-derived mesenchymal stem cells, containing CeO_2 NPs, counter oxidative damage and promote tendon regeneration [31].

Mesenchymal stem cells (MSCs) are a promising resource for various biomedical applications, including those associated with tissue regeneration and cancer treatment. The ability of MSCs to migrate to areas of injury and inflammation

makes them an effective delivery vehicle for various functionalized nanomaterials to the sites of injury [32], inflammation [33] or into tumor growth area [34, 35], providing a pronounced therapeutic effect. MSCs fully exhibit their immunomodulatory properties only when they are in a specific microenvironment, which forms their tissue niche *in vivo* [36]. The most promising approach to ensure their optimal characteristics is through three-dimensional cell cultivation in cellular spheroids, as opposed to two-dimensional cultures [37–40]. In 3D structures, MSCs are able to form contacts and exchange regulatory signals with each other, as well as to produce an extracellular matrix that contributes to their function. However, the presence of the extracellular matrix can affect the efficiency of nanoparticles penetration into these structures [41–44]. Earlier, it was shown in a model of cellular spheroids formed from human umbilical vein endothelial cells (HUVEC) and MSCs, that nanoceria-decorated graphene oxide (CeGO) could be used for the treatment of critical limb ischemia [45]. CeGO uptake enhanced the survival rate and anti-apoptotic capacity of cellular spheroids, upregulated expression of angiogenic markers, ensuring high cell survival rate. Thus, the use of cerium-containing nanoparticles shows high promise in maintaining normal functioning of cell spheroids formed from mesenchymal stem cells [31, 46–48].

Additional functionalization of CeO_2 NPs makes it possible to develop effective therapeutic agents exhibiting new functional properties that ensure their tracking both inside cells and in tissues. In particular, it has previously been shown that doping of CeO_2 NPs with gadolinium ions allows for their visualization using magnetic resonance imaging [27]. McDonagh et al. developed a single-pot synthesis of CeO_2 NPs modified with zirconium-89 isotope allowing detailed PET imaging and *ex vivo* biodistribution visualization of CeO_2 NPs [49]. The potential of modifying nanoparticles with carbon dots has also been demonstrated [50]. Zhang et al. synthesized a new type of carbon material doped with cerium (Ce–Cd), using a simple hydrothermal process. This material exhibited pronounced luminescent properties and high photostability. It also possessed biological activity, as demonstrated by its antibacterial and wound-healing properties.

In this study, we performed additional functionalization of gadolinium-doped ceria NPs with a fluorescent tag and conducted a comprehensive assessment of their cytotoxic effects. We further analyzed the specific features of internalization of these multifunctional NPs into mesenchymal stem cells cultured in monolayers (2D system) and cellular spheroids (3D system).

2. Materials and methods

2.1. Synthesis procedure

$Ce_{0.8}Gd_{0.2}O_{2-x}$ NPs were synthesized according to a recently reported procedure [51]. Briefly, a mixed solution of cerium(III) and gadolinium(III) nitrates (0.18 and 0.02 M, respectively) and dextran (Mr $\approx$ 6000) was prepared, with the ($Ce(NO_3)_3 \cdot 6H_2O$ + $Gd(NO_3)_3 \cdot 6H_2O$):dextran ratio being 1:2 (wt). To the continuously stirred solution, 1 M aqueous ammonia was added dropwise for 3 h, maintaining the pH at 7.5 – 8.0. When pH became constant, the mixture was stirred again, for 2 h, and then aqueous ammonia was added to achieve pH = 12, followed by additional stirring for 8 h. To the sol obtained, an excess of isopropanol was added and the mixture was refluxed to form a white precipitate. The precipitate was further washed with hot isopropanol several times and dried in air at 60 °C. Gadolinium-doped ceria sol was prepared by dispersing the powder in deionized water. $Ce_{0.8}Gd_{0.2}O_{2-x}$ NPs were functionalized using fluorescein isothiocyanate (FITC) to make it possible to study their intracellular localization. The dry powder of dextran-stabilized $Ce_{0.8}Gd_{0.2}O_{2-x}$ nanoparticles (3 g) was added to 20 mL of anhydrous dimethyl sulfoxide (DMSO) and 0.5 mL of pyridine. The mixture was then stirred for four hours at 95 °C until it was completely dissolved. Afterwards, 100 mg of FITC were added to the solution and the mixture was allowed to continue to mix for 2 hours in the dark. Following this, 50 mL of isopropanol was added to the resultant solution. The resulting mixture was then centrifuged at 10,000 g for 10 minutes. The precipitate that formed was repeatedly washed until the color in the supernatant had disappeared, and then it was dried at 60 °C in the dark to a constant mass. The dry powder of FITC-$Ce_{0.8}Gd_{0.2}O_{2-x}$ NPs was stored at 4 °C.

2.2. Characterization of FITC-$Ce_{0.8}Gd_{0.2}O_{2-x}$ NPs

The size and shape of FITC-$Ce_{0.8}Gd_{0.2}O_{2-x}$ NPs were analysed by transmission electron microscopy (TEM) using a Leo912 AB Omega electron microscope equipped with an electron energy loss spectrometer (EELS) operating at an accelerating voltage of 100 kV. The study of the chemical composition of the obtained materials was carried out using energy dispersive X-ray spectroscopy (EDX) using a Tescan Amber GMH microscope equipped with an Ultim MAX detector with 100 mm^2 active area (Oxford Instruments) at an accelerating voltage of 20 kV. EDX data were processed using the AZtec software (5.0). The concentration of the $Ce_{0.8}Gd_{0.2}O_{2-x}$ NPs (without FITC) sols was measured gravimetrically. The corundum crucibles, pre-annealed at 900 °C for 2 hours, were weighed on analytical scales to establish their initial weight. Then 3 mL of sol was placed in each crucible and heated in a muffle furnace at 900 °C for 2 hours with slow heating ($\sim$ 3 °/min). After cooling to room temperature, the crucibles were weighed. The weight of the dry residue of the annealing product was determined and the concentration of the initial sols was calculated. A DS-11+ spectrophotometer (DeNOVIX, USA) was used to measure FITC-$Ce_{0.8}Gd_{0.2}O_{2-x}$ sols absorbance in the UV-visible range. Measurements were carried out in the wavelength range from 200 to 500 nm in 0.1 nm increments. The hydrodynamic size, PDI and ζ-potential of the nanoparticles were determined by dynamic and electrophoretic light scattering at 25 °C using a BeNano analyzer (BetterSize, Dandong, China).

2.3. Cell culture

The experiments were performed using human mesenchymal stem cells (hMSCs). hMSCs were isolated from the pulp of a third molar extracted for orthodontic reasons from a healthy 12-year-old patient (with his written consent). All the experiments were carried out in agreement with good clinical practice and the ethical principles stated in the current edition of the Declaration of Helsinki. Cells were cultured in DMEM/F12 medium (1:1) (PanEko, Moscow, Russia) supplemented with L-glutamine (146 mg per 450 mL of medium) (PanEko, Moscow, Russia), penicillin, streptomycin (PanEko, Moscow, Russia), and 10 % fetal bovine serum (Biosera, Cholet, France). Cultivation was carried out in culture flasks with filter caps with a cultivation area of 25 and 75 cm^2 (TPP, Trasadingen, Switzerland) in a CO_2 incubator with a CO_2 concentration of 5 % at a temperature of 37 °C.

2.4. MTT assay

Cell metabolic activity was assessed using MTT assay which is based on the reduction of a yellow tetrazolium salt (3-[4,5-dimethylthiazole-2-yl]-2,5-diphenyl tetrazolium bromide, MTT) with the formation of insoluble purple formazan. After 48 hours of cultivation, 0.5 mg/mL MTT reagent solution, dissolved in culture medium without FBS, was added to the wells. The optical density of the formed formazan was measured at $\lambda = 570$ nm using an INNO-S plate reader (LTEK, Korea).

2.5. Measuring of mitochondrial membrane potential

The mitochondrial membrane potential (MMP) was measured by staining cells with TMRE (tetramethylrhodamine, ethyl ester, ThermoFisher, Carlsbad, CA, USA) fluorescent dye followed by fluorescence microscopy analysis. After 24, 48, and 72 hours of incubation with nanoparticles, the culture medium was replaced with TMRE solution in Hanks' buffer (PanEko, Moscow, Russia). After 15 min of incubation with dye, the cells were washed three times with Hanks' buffer solution. Then the cells were photographed using a ZOE fluorescent imager (Bio-Rad, USA). TMRE fluorescence intensity, which directly correlates with the MMP of cells, was measured using the ImageJ software. For statistics, three different areas in three different microphotographs were analyzed. Quantitative analysis results were presented as mean $\pm$ SD.

2.6. Cell proliferation analysis

The analysis of proliferative activity was carried out by examining the confluence of cell culture during 72 hours of coincubation with FITC-$Ce_{0.8}Gd_{0.2}O_{2-x}$ NPs. The cells were monitored in real time using JULI-stage live cell imaging system (NanoEntek, Korea). Confluence growth curves were plotted using the GraphPad Prism 8 software.

2.7. Spheroid formation

Cellular spheroids were prepared using the "hanging drop" technique. hMSCs were removed from the substrate by using a trypsin-EDTA solution (0.05 %) and then washed three times by centrifugation at 1,000 RPM for 5 minutes. Next, DMEM/F12 growth medium with 10 % fetal bovine serum (FBS) was added to the cells. Subsequently, methylcellulose (1 % in DMEM/F12 medium) was added to the cell suspension to ensure that the total concentration of methyl cellulose did not exceed 0.25 %. The concentration of hMSCs used was 125,000 cells/mL. The cells were seeded to form spheroid onto the lid of a 60-mm plastic Petri dish in drops of 20 μl volume. To prevent desiccation of the drops, a 10-ml Hanks buffer was positioned at the bottom of the dish. Afterwards, the lid of the dish was carefully positioned on top and incubated for 72 hours in a CO_2 incubator. After 24 hours of incubation, the cells had aggregated in the center of the drop, forming a spherical structure.

2.8. Uptake analysis of FITC-$Ce_{0.8}Gd_{0.2}O_{2-x}$ NPs

The cell uptake analysis of FITC-$Ce_{0.8}Gd_{0.2}O_{2-x}$ NPs in the hMSCs' 2D and 3D systems was carried out using fluorescence microscopy with a Celena S cell imager (Logos, Korea) and a Zoe cell imager (Bio RAD, USA). The cells were seeded at a density of 104 cells per cm^2 into a 35 mm Petri dish with a central hole. After that, FITC-$Ce_{0.8}Gd_{0.2}O_{2-x}$ NPs and the cells were added and cultivated for 0.5 – 16 hours.

2.9. Statistical analysis

The data were analyzed using the GraphPad Prism 8 software. The statistical significance of the deviations between the test sets and the control was confirmed using the Welch t-test. Images were processed using ImageJ and Adobe Photoshop software.

3. Results and discussion

Previously reported procedure of the $Ce_{0.8}Gd_{0.2}O_{2-x}$ NPs synthesis [52] was modified: FITC was used as an additional fluorescent label. Fig. 1a shows the appearance of nanoparticles in the form of dried powder (left) and in the form of colloidal solution (right). TEM image (Fig. 1b) confirms the formation of the individual nanoparticles with a mean size of 3 nm. According to full-profile analysis of the diffraction pattern, the crystal lattice parameter of the FITC-$Ce_{0.8}Gd_{0.2}O_{2-x}$ NPs is equal to 5.425(1) Å. This value differs significantly from ceria lattice parameter, 5.411 Å (PDF2 #00-034-394) indicating the formation of a nanocrystalline solid solution; the calculated value corresponds well with the previous experimental data on the dependence of the NPs lattice parameter on gadolinium content [53]. The chemical composition of the nanoparticles was additionally confirmed by EDX analysis (Fig. 1c). ζ-potential of the FITC-$Ce_{0.8}Gd_{0.2}O_{2-x}$ NPs in deionized water was 11.3 ± 1.2 mV (Fig. 1d). UV/visible spectrum is presented in Fig. 1e. FITC-$Ce_{0.8}Gd_{0.2}O_{2-x}$ NPs exhibited excellent colloidal stability in aqueous media: the hydrodynamic size of the FITC-$Ce_{0.8}Gd_{0.2}O_{2-x}$ NPs is 6.18 nm with polydispersity index (PDI) $= 0.44$ (Fig. 1f).

CeO_2 NPs have a high degree of biocompatibility [54–56]. In turn, one of the challenges associated with the biomedical use of gadolinium-containing nanoparticles is the potential for uncontrolled release of gadolinium ions into the cell during the dissolution of the nanoparticles. This can lead to a pronounced cytotoxic effect [57–60]. We have previously demonstrated that Gd-doped CeO_2 NPs did not release toxic gadolinium ions due to the extremely low solubility of ceria matrix [52]. FITC-$Ce_{0.8}Gd_{0.2}O_{2-x}$ NPs also show a high degree of biocompatibility towards hMSCs in a wide range of

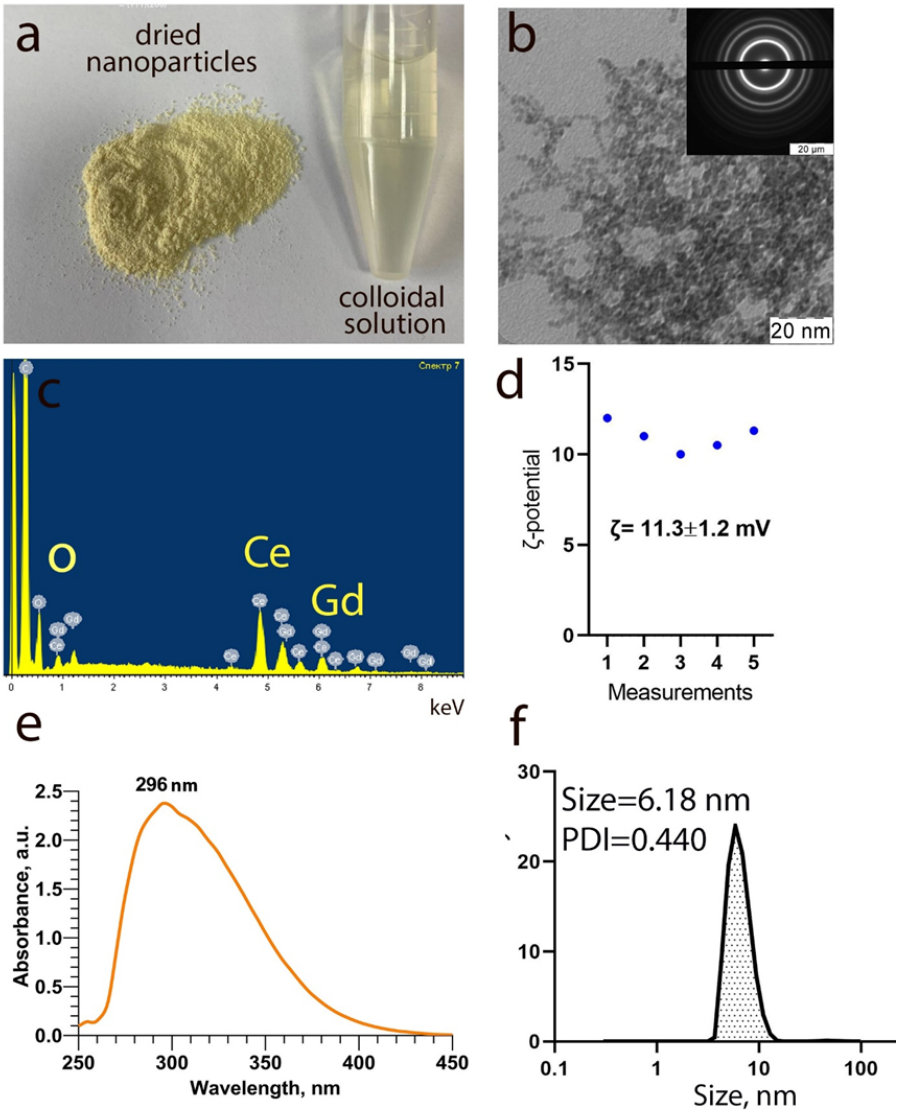

FIG. 1. Visual appearance of dried FITC-$Ce_{0.8}Gd_{0.2}O_{2-x}$ NPs and the corresponding colloidal solution (a), transmission electron microscopy and selected area electron diffraction (in the inset) (b), EDX analysis (c), ζ-potential distribution in MQ water (d), UV-visible absorbance spectrum (e) hydrodynamic size distribution and PDI (f) of the NPs

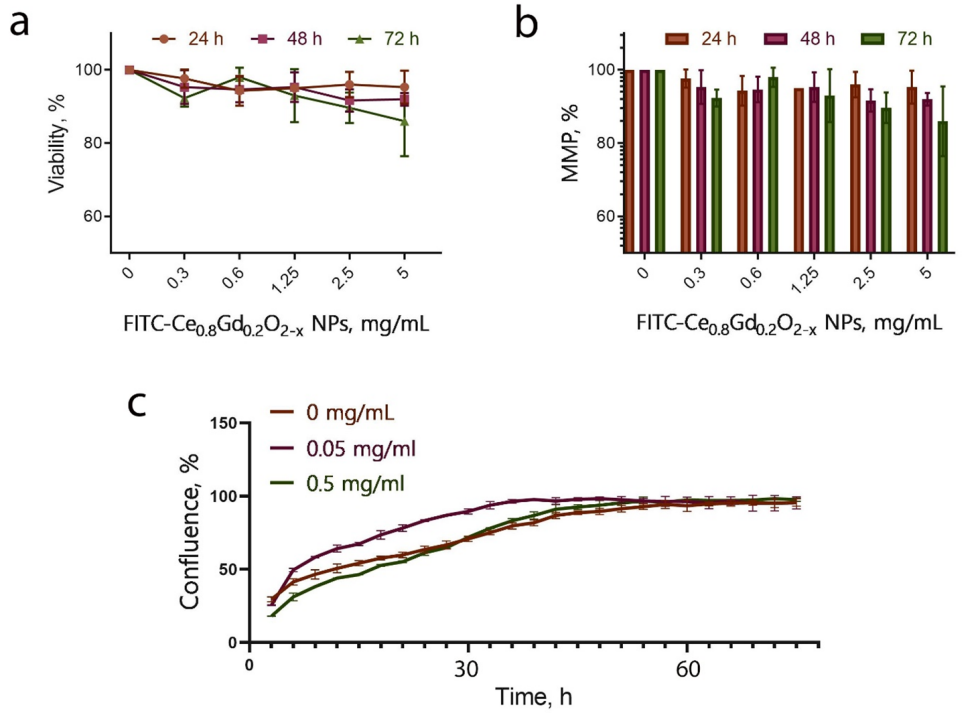

FIG. 2. Cell viability (MTT assay), membrane mitochondrial potential analysis (TMRE staining) and analysis of cell proliferation (JuliStage imaging) of hMSCs after incubation with FITC-$Ce_{0.8}Gd_{0.2}O_{2-x}$ NPs in a wide range of concentrations (0 – 5 mg/mL)

concentrations, up to 5 mg/mL (Fig. 2). Preincubation of the cells with these nanoparticles does not result in a decrease of their metabolic activity (via MTT assay) even at high concentrations (2.5 –5 mg/mL) after 24, 48, and 72 hours of incubation (Fig. 2a). Analysis of the effect of FITC-$Ce_{0.8}Gd_{0.2}O_{2-x}$ NPs on MMP revealed no decrease in hMSCs' membrane potential in the same concentration range, confirming the high degree of nanoparticles biocompatibility (Fig. 2b). hMSCs proliferation was also assessed after incubation with nanoparticles at concentrations of 0.05 and 0.5 mg/mL, with no statistically significant decrease in cell proliferation rate observed for these concentrations of nanoparticles (Fig. 2c). Therefore, FITC-$Ce_{0.8}Gd_{0.2}O_{2-x}$ NPs do not exhibit any observable cytotoxic effects on hMSCs *in vitro*.

Earlier, CeO_2 NPs were shown to possess brilliant antioxidant properties in various biomedical applications. However, the interaction peculiarities of CeO_2 NPs with cells and their intracellular localization are still poorly understood. It has previously been demonstrated that the efficiency of the cellular uptake and accumulation of CeO_2 NPs depends strongly on their size, charge, shape and concentration [23, 61, 62]. In particular, CeO_2 NPs with a positive or neutral charge are internalized into normal and cancer cells, while CeO_2 NPs with a negative charge are internalized mainly by cancer cell lines [63–65]. This fact was also confirmed in a study by Zhou et al. which showed that negatively charged CeO_2 NPs were predominantly absorbed by lung adenocarcinoma cells (A549) [66]. They attributed this observation to the different efficiencies of protein absorption on the surface of nanoparticles and the formation of different protein coronas [67, 68]. Moreover, when entering cells, CeO_2 NPs are localized in different cellular compartments (for example, in the cytoplasm and in lysosomes), depending on the surface charge of the nanoparticle. The internalization and sub-cellular localization of CeO_2 NPs play a key role in the cytotoxic profile of nanoparticles, with significant toxicity shown when they are located in lysosomes [63]. Here, we have studied the accumulation process of FITC-$Ce_{0.8}Gd_{0.2}O_{2-x}$ NPs in the 2D cell culture of hMSCs (Fig. 3). For this purpose, cell nuclei were stained with a fluorescent dye, Hoechst 33342 (blue fluorescence), to counterstain and to visualize the accumulation of FITC-$Ce_{0.8}Gd_{0.2}O_{2-x}$ NPs (green fluorescence) in the cell cytoplasm. Fig. 3a shows the images of hMSCs 0.5 – 16 hours after treatment with FITC-$Ce_{0.8}Gd_{0.2}O_{2-x}$ NPs. It is clearly seen that the nanoparticles are predominantly localized in the cytoplasm and partially in lysosomes after 16 hours of incubation. The lysosomal localization is confirmed by the presence of bright green zones in the cells cytoplasm. The quantitative assessment of FITC-$Ce_{0.8}Gd_{0.2}O_{2-x}$ NPs internalization is presented in Fig. 3b.

The analysis of the internalization of nanoparticles into cellular spheroids is more interesting, as the more developed intercellular contacts and three-dimensional cell arrangement play a special role in this process [41]. Consequently, a 3D cell arrangement is a more adequate model of biological tissue in vitro than a 2D cell monolayer. Multicellular spheroids closely mimic the physiological microenvironment of individual cells [69]. The structure of cellular spheroids with a diameter larger than 300 micrometers is usually represented by several distinct zones, including a necrosis zone,

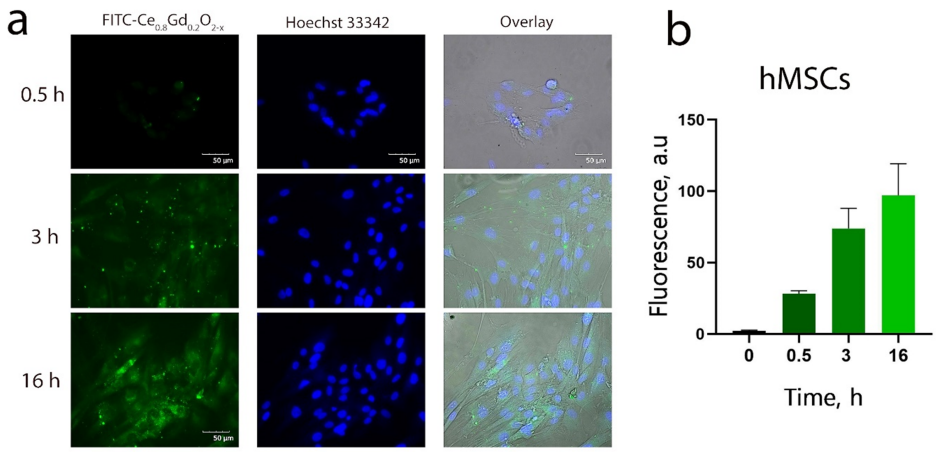

FIG. 3. Cellular uptake analysis of FITC-$Ce_{0.8}Gd_{0.2}O_{2-x}$ NPs in 2D cell cultures of hMSCs. Nanoparticles were introduced at a concentration of 10 μg/mL and co-incubated with cells for 3, 6 and 16 hours

hypoxia zone, and proliferation zone [70]. These zones have specific physiological characteristics and vary in pH value, proliferative activity of cells and degree of hypoxia [71].

We have demonstrated that FITC-$Ce_{0.8}Gd_{0.2}O_{2-x}$ NPs are able to internalize cellular spheroids formed from hMSCs effectively (Fig. 4). Within 30 minutes, FITC-$Ce_{0.8}Gd_{0.2}O_{2-x}$ NPs are internalized 20 – 30 micrometers deep into cellular spheroids. This means that the nanoparticles are localized in the proliferation zone. However, after 5 hours, the penetration depth increased up to 120 – 150 micrometers. 12 hours of incubation resulted in the highest uptake of FITC-$Ce_{0.8}Gd_{0.2}O_{2-x}$ NPs into cellular spheroids. Thus, it can be concluded that FITC-$Ce_{0.8}Gd_{0.2}O_{2-x}$ nanoparticles are able to accumulate effectively in cellular spheroids, and remain there for more than 48 hours of co-cultivation.

4. Conclusion

Multi-functional FITC-$Ce_{0.8}Gd_{0.2}O_{2-x}$ NPs were synthesized and characterized in detail by relevant physical techniques. The nanoparticles are not toxic to hMSCs at concentrations up to 5 mg/mL, maintaining a high level of cell viability, metabolic and proliferative activity. In 30 minutes, FITC-$Ce_{0.8}Gd_{0.2}O_{2-x}$ NPs effectively internalize into cellular monolayer of hMSCs and their maximum accumulation occurs after 16 hours. The FITC-$Ce_{0.8}Gd_{0.2}O_{2-x}$ NPs are also effectively internalized into 3D cellular spheroids after 12 hours without causing toxicity or disrupting their structure. The results obtained indicate that the use of cerium-based nanoparticles is a promising approach for the safe and efficient visualization of hMSCs that could be used in tissue engineering and regenerative medicine, such as in 3D bioprinting.

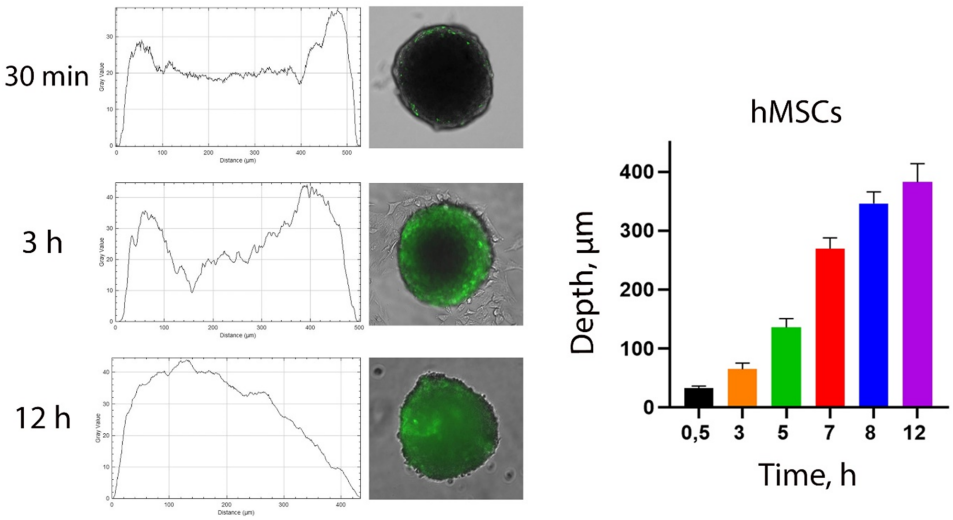

FIG. 4. Accumulation of FITC-$Ce_{0.8}Gd_{0.2}O_{2-x}$ in 3D cellular spheroids formed from hMSCs. Nanoparticles were introduced at a concentration of 10 μg/mL and co-incubated with cell spheroids for 12 hours

References

[1] Feng N., Liu Y., Dai X., Wang Y., Guo Q., Li Q. Advanced Applications of Cerium Oxide Based Nanozymes in Cancer. *RSC Adv.*, 2022, **12**, P. 121486–1493.

[2] Saifi M.A., Seal S., Godugu C. Nanoceria, the Versatile Nanoparticles: Promising Biomedical Applications. *J. Controlled Release*, 2021, **338**, P. 164–189.

[3] Tang J.L.Y., Moonshi S.S., Ta H.T. Nanoceria: An Innovative Strategy for Cancer Treatment. *Cell. Mol. Life Sci.*, 2023, **80**, 46.

[4] Xue Y., Yang F., Wu L., Xia D., Liu Y. CeO_2 Nanoparticles to Promote Wound Healing: A Systematic Review. *Adv. Healthc. Mater.*, 2024, **13** (6), 2302858.

[5] Shcherbakov A.B., Ivanov V.K., Zholobak N.M., Ivanova O.S., Krysanov E.Yu., Baranchikov A.E., Spivak N.Ya., Tretyakov Yu.D. Nanocrystalline Ceria Based Materials—Perspectives for Biomedical Application. *Biophysics*, 2011, **56**, P. 987–1004.

[6] Hirst S.M., Karakoti A.S., Tyler R.D., Sriranganathan N., Seal S., Reilly C.M. Anti-Inflammatory Properties of Cerium Oxide Nanoparticles. *Small Weinh. Bergstr. Ger.*, 2009, **5**, P. 2848–2856.

[7] Heckert E., Karakoti A., Seal S., Self W.T. The Role of Cerium Redox State in the SOD Mimetic Activity of Nanoceria. *Biomaterials*, 2008, **29**, P. 2705–2709.

[8] Baldim V., Bedioui F., Mignet N., Margaill I., Berret J.-F. The Enzyme-like Catalytic Activity of Cerium Oxide Nanoparticles and Its Dependency on Ce^{3+} Surface Area Concentration. *Nanoscale*, 2018, **10**, P. 6971–6980.

[9] Pirmohamed T., Dowding J.M., Singh S., Wasserman B., Heckert E., Karakoti A.S., King J.E.S., Seal S., Self W.T. Nanoceria Exhibit Redox State-Dependent Catalase Mimetic Activity. *Chem. Commun. Camb. Engl.*, 2010, **46**, P. 2736–2738.

[10] Dhall A., Burns A., Dowding J., Das S., Seal S., Self W. Characterizing the Phosphatase Mimetic Activity of Cerium Oxide Nanoparticles and Distinguishing Its Active Site from That for Catalase Mimetic Activity Using Anionic Inhibitors. *Environ. Sci. Nano*, 2017, **4**, P. 1742–1749.

[11] Hu H., Kang X., Shan Z., Yang X., Bing W., Wu L., Ge H., Ji H. A DNase-Mimetic Artificial Enzyme for the Eradication of Drug-Resistant Bacterial Biofilm Infections. *Nanoscale*, 2022, **14**, P. 2676–2685.

[12] Sozarukova M.M., Proskurnina E.V., Popov A.L., Kalinkin A.L., Ivanov V.K. New Facets of Nanozyme Activity of Ceria: Lipo- and Phospholipoperoxidase-like Behaviour of CeO_2 Nanoparticles. *RSC Adv.*, 2021, **11**, P. 35351–35360.

[13] Wang G., Zhang J., He X., Zhang Z., Zhao Y. Ceria Nanoparticles as Enzyme Mimetics. *Chin. J. Chem.*, 2017, **35**, P. 791–800.

[14] Wang Z., Shen X., Gao X., Zhao Y. Simultaneous Enzyme Mimicking and Chemical Reduction Mechanisms for Nanoceria as a Bio-Antioxidant: A Catalytic Model Bridging Computations and Experiments for Nanozymes. *Nanoscale*, 2019, **11**, P. 13289–13299.

[15] Sozarukova M.M., Chilikina P.A., Novikov D.O., Proskurnina E.V., Baranchikov A.E., Ivanov V.K. Cerium Dioxide Nanoparticles Modulate the Oxidative Metabolism of Neutrophils upon Blood Irradiation with a Pulsed Broadband UV Source. *Nanosyst. Phys. Chem. Math.*, 2023, **14**, P. 644–651.

[16] Ivanov V.K., Polezhaeva O.S., Tret'yakov Yu.D. Nanocrystalline Ceria: Synthesis, Structure-Sensitive Properties, and Promising Applications. *Russ. J. Gen. Chem.*, 2010, **80**, P. 604–617.

[17] Naganuma T., Traversa E. Stability of the Ce^{3+} Valence State in Cerium Oxide Nanoparticle Layers. *Nanoscale*, 2012, **4**, P. 4950–4953.

[18] Naganuma T., Traversa E. The Effect of Cerium Valence States at Cerium Oxide Nanoparticle Surfaces on Cell Proliferation. *Biomaterials*, 2014, **35**, P. 4441–4453.

[19] Popov A.L., Shcherbakov A.B., Zholobak N.M., Baranchikov A.E., Ivanov V.K. Cerium Dioxide Nanoparticles as Third-Generation Enzymes (Nanozymes). *Nanosyst. Phys. Chem. Math.*, 2017, P. 760–781.

[20] Gao R., Mitra R.N., Zheng M., Wang K., Dahringer J.C., Han Z. Developing Nanoceria-Based pH-Dependent Cancer-Directed Drug Delivery System for Retinoblastoma. *Adv. Funct. Mater.*, 2018, **28**, 1806248.

[21] Xu C., Lin Y., Wang J., Wu L., Wei W., Ren J., Qu X. Nanoceria-Triggered Synergetic Drug Release Based on CeO_2-Capped Mesoporous Silica Host–Guest Interactions and Switchable Enzymatic Activity and Cellular Effects of CeO_2. *Adv. Healthc. Mater.*, 2013, **2**, P. 1591–1599.

[22] Zholobak N.M., Ivanov V.K., Shcherbakov A.B. Chapter 12 -0 Interaction of Nanoceria with Microorganisms. In *Nanobiomaterials in Antimicrobial Therapy*, Grumezescu A.M., Ed., William Andrew Publishing, 2016, P. 419–450.

[23] Singh S., Ly A., Das S., Sakthivel T.S., Barkam S., Seal S. Cerium Oxide Nanoparticles at the Nano-Bio Interface: Size-Dependent Cellular Uptake. *Artif. Cells Nanomedicine Biotechnol.*, 2018, **46**, P. 956–963.

[24] Lim S., Kim W., Song S., Shim M.K., Yoon H.Y., Kim B.-S., Kwon I.C., Kim K. Intracellular Uptake Mechanism of Bioorthogonally Conjugated Nanoparticles on Metabolically Engineered Mesenchymal Stem Cells. *Bioconjug. Chem.*, 2021, **32**, P. 199–214.

[25] Popov A.L., Popova N.R., Selezneva I.I., Akkizov A.Y., Ivanov V.K. Cerium Oxide Nanoparticles Stimulate Proliferation of Primary Mouse Embryonic Fibroblasts in Vitro. *Mater. Sci. Eng. C*, 2016, **68**, P. 406–413.

[26] Mahapatra C., Singh R.K., Lee J.-H., Jung J., Hyun J.K., Kim H.-W. Nano-Shape Varied Cerium Oxide Nanomaterials Rescue Human Dental Stem Cells from Oxidative Insult through Intracellular or Extracellular Actions. *Acta Biomater.*, 2017, **50**, P. 142–153.

[27] Popov A.L., Savintseva I.V., Kozlova T.O., Ivanova O.S., Zhukov I.V., Baranchikov A.E., Yurkovskaya A.V., Savelov A.A., Ermakov A.M., Popova N.R., et al. Heavily Gd-Doped Non-Toxic Cerium Oxide Nanoparticles for MRI Labelling of Stem Cells. *Molecules*, 2023, **28**, 1165.

[28] Popov A.L., Ermakov A.M., Savintseva I.V., Selezneva I.I., Poltavtseva R.A., Zaraisky E.I., Poltavtsev A.M., Stepanov A.A., Ivanov V.K., Sukhikh G.T. Citrate-stabilized nanoparticles of CeO_2 stimulate proliferation of human mesenchymal stem cells IN VITRO. *Nanosci. Technol. Int. J.*, 2016, **7**.

[29] Nilawar S., Chatterjee K. Surface Decoration of Redox-Modulating Nanoceria on 3D-Printed Tissue Scaffolds Promotes Stem Cell Osteogenesis and Attenuates Bacterial Colonization. *Biomacromolecules*, 2022, **23**, P. 226–239.

[30] Rather H.A., Thakore R., Singh R., Jhala D., Singh S., Vasita R. Antioxidative Study of Cerium Oxide Nanoparticle Functionalised PCL-Gelatin Electrospun Fibers for Wound Healing Application. *Bioact. Mater.*, 2018, **3**, P. 201–211.

[31] Ren X., Zhuang H., Zhang Y., Zhou P. Cerium Oxide Nanoparticles-Carrying Human Umbilical Cord Mesenchymal Stem Cells Counteract Oxidative Damage and Facilitate Tendon Regeneration. *J. Nanobiotechnology*, 2023, **21**, 359.

[32] D'Atri D., Zerrillo L., Garcia J., Oieni J., Lupu-Haber Y., Schomann T., Chan A., Cruz L.J., Creemers L.B., Machluf M. Nanoghosts: Mesenchymal Stem Cells Derived Nanoparticles as a Unique Approach for Cartilage Regeneration. *J. Controlled Release*, 2021, **337**, P. 472–481.

[33] Li X., Wei Z., Zhang W., Lv H., Li J., Wu L., Zhang H., Yang B., Zhu M., Jiang J. Anti-Inflammatory Effects of Magnetically Targeted Mesenchymal Stem Cells on Laser-Induced Skin Injuries in Rats. *Int. J. Nanomedicine*, 2020, **15**, P. 5645–5659.

[34] Gao Z., Zhang L., Hu J., Sun Y. Mesenchymal Stem Cells: A Potential Targeted-Delivery Vehicle for Anti-Cancer Drug, Loaded Nanoparticles. *Nanomedicine Nanotechnol. Biol. Med.*, 2013, **9**, P. 174–184.

[35] Roger M., Clavreul A., Venier-Julienne M.-C., Passirani C., Sindji L., Schiller P., Montero-Menei C., Menei P. Mesenchymal Stem Cells as Cellular Vehicles for Delivery of Nanoparticles to Brain Tumors. *Biomaterials*, 2010, **31**, P. 8393–8401.

[36] Amiri F., Jahanian-Najafabadi A., Roudkenar M.H. In Vitro Augmentation of Mesenchymal Stem Cells Viability in Stressful Microenvironments. *Cell Stress Chaperones*, 2015, **20**, P. 237–251.
[37] Białkowska K., Komorowski P., Bryszewska M., Miłowska K. Spheroids as a Type of Three-Dimensional Cell Cultures—Examples of Methods of Preparation and the Most Important Application. *Int. J. Mol. Sci.*, 2020, **21**, 6225.
[38] Zanoni M., Piccinini F., Arienti C., Zamagni A., Santi S., Polico R., Bevilacqua A., Tesei A. 3D Tumor Spheroid Models for in Vitro Therapeutic Screening: A Systematic Approach to Enhance the Biological Relevance of Data Obtained. *Sci. Rep.*, 2016, **6**, 19103.
[39] Kim W., Gwon Y., Park S., Kim H., Kim J. Therapeutic Strategies of Three-Dimensional Stem Cell Spheroids and Organoids for Tissue Repair and Regeneration. *Bioact. Mater.*, 2023, **19**, P. 50–74.
[40] Wang W., Itaka K., Ohba S., Nishiyama N., Chung U., Yamasaki Y., Kataoka K. 3D Spheroid Culture System on Micropatterned Substrates for Improved Differentiation Efficiency of Multipotent Mesenchymal Stem Cells. *Biomaterials*, 2009, **30**, P. 2705–2715.
[41] Tchoryk A., Taresco V., Argent R.H., Ashford M., Gellert P.R., Stolnik S., Grabowska A., Garnett M.C. Penetration and Uptake of Nanoparticles in 3D Tumor Spheroids. *Bioconjug. Chem.*, 2019, **30**, P. 1371–1384.
[42] Roy S.M., Garg V., Barman S., Ghosh C., Maity A.R., Ghosh S.K. Kinetics of Nanomedicine in Tumor Spheroid as an In Vitro Model System for Efficient Tumor-Targeted Drug Delivery With Insights From Mathematical Models. *Front. Bioeng. Biotechnol.*, 2021, **9**.
[43] Zhuang J., Zhang J., Wu M., Zhang Y. A Dynamic 3D Tumor Spheroid Chip Enables More Accurate Nanomedicine Uptake Evaluation. *Adv. Sci.*, 2019, **6**, 1901462.
[44] Sokolova V., Ebel J.-F., Kollenda S., Klein K., Kruse B., Veltkamp C., Lange C.M., Westendorf A.M., Epple M. Uptake of Functional Ultrasmall Gold Nanoparticles in 3D Gut Cell Models. *Small*, 2022, **18**, 2201167.
[45] Bayaraa O., Dashnyam K., Singh R.K., Mandakhbayar N., Lee J.H., Park J.-T., Lee J.-H., Kim H.-W. Nanoceria-GO-Intercalated Multicellular Spheroids Revascularize and Salvage Critical Ischemic Limbs through Anti-Apoptotic and pro-Angiogenic Functions. *Biomaterials*, 2023, **292**, 121914.
[46] Liu D., Lu G., Shi B., Ni H., Wang J., Qiu Y., Yang L., Zhu Z., Yi X., Du X., et al. ROS-Scavenging Hydrogels Synergize with Neural Stem Cells to Enhance Spinal Cord Injury Repair via Regulating Microenvironment and Facilitating Nerve Regeneration. *Adv. Healthc. Mater.*, 2023, **12**, 2300123.
[47] Liu D.-D., Zhang J.-C., Zhang Q., Wang S.-X., Yang M.-S. TGF-β/BMP Signaling Pathway Is Involved in Cerium-Promoted Osteogenic Differentiation of Mesenchymal Stem Cells. *J. Cell. Biochem.*, 2013, **114**, P. 1105–1114.
[48] Yin P., Liang W., Han B., Yang Y., Sun D., Qu X., Hai Y., Luo D. Hydrogel and Nanomedicine-Based Multimodal Therapeutic Strategies for Spinal Cord Injury. *Small Methods*, 2024, **8**, 2301173.
[49] McDonagh P.R., Sundaresan G., Yang L., Sun M., Mikkelsen R., Zweit J. Biodistribution and PET Imaging of 89-Zirconium Labeled Cerium Oxide Nanoparticles Synthesized with Several Surface Coatings. *Nanomedicine Nanotechnol. Biol. Med.*, 2018, **14**, P. 1429–1440.
[50] Zhang M., Zhai X., Ma T., Huang Y., Yan C., Du Y. Multifunctional Cerium Doped Carbon Dots Nanoplatform and Its Applications for Wound Healing. *Chem. Eng. J.*, 2021, **423**, 130301.
[51] Shcherbakov A.B., Zholobak N.M., Ivanov V.K., Ivanova O.S., Marchevsky A.V., Baranchikov A.E., Spivak N.Ya., Tretyakov Yu.D. Synthesis and Antioxidant Activity of Biocompatible Maltodextrin-Stabilized Aqueous Sols of Nanocrystalline Ceria. *Russ. J. Inorg. Chem.*, 2012, **57**, P. 1411–1418.
[52] Popov A.L., Abakumov M.A., Savintseva I.V., Ermakov A.M., Popova N.R., Ivanova O.S., Kolmanovich D.D., Baranchikov A.E., Ivanov V.K. Biocompatible Dextran-Coated Gadolinium-Doped Cerium Oxide Nanoparticles as MRI Contrast Agents with High T1 Relaxivity and Selective Cytotoxicity to Cancer Cells. *J. Mater. Chem. B*, 2021, **9**, P. 6586–6599.
[53] Dolgopolova E.A., Ivanova O.S., Ivanov V.K., Sharikov F.Yu., Baranchikov A.E., Shcherbakov A.B., Trietyakov Yu.D. Microwave-Hydrothermal Synthesis of Gadolinium-Doped Nanocrystalline Ceria in the Presence of Hexamethylenetetramine. *Russ. J. Inorg. Chem.*, 2012, **57**, P. 1303–1307.
[54] Aalapati S., Ganapathy S., Manapuram S., Anumolu G., Prakya B.M. Toxicity and Bio-Accumulation of Inhaled Cerium Oxide Nanoparticles in CD1 Mice. *Nanotoxicology*, 2014, **8**, P. 786–798.
[55] Hirst S.M., Karakoti A., Singh S., Self W., Tyler R., Seal S., Reilly C.M. Bio-Distribution and in Vivo Antioxidant Effects of Cerium Oxide Nanoparticles in Mice. *Environ. Toxicol.*, 2013, **28**, P. 107–118.
[56] Nosrati H., Heydari M., Khodaei M. Cerium Oxide Nanoparticles: Synthesis Methods and Applications in Wound Healing. *Mater. Today Bio*, 2023, **23**, 100823.
[57] Akhtar M.J., Ahamed M., Alhadlaq H., Alrokayan S. Toxicity Mechanism of Gadolinium Oxide Nanoparticles and Gadolinium Ions in Human Breast Cancer Cells. *Curr. Drug Metab.*, 2019, **20**, P. 907–917.
[58] Rogosnitzky M., Branch S. Gadolinium-Based Contrast Agent Toxicity: A Review of Known and Proposed Mechanisms. *BioMetals*, 2016, **29**, P. 365–376.
[59] Takanezawa Y., Nakamura R., Kusaka T., Ohshiro Y., Uraguchi S., Kiyono M. Significant Contribution of Autophagy in Mitigating Cytotoxicity of Gadolinium Ions. *Biochem. Biophys. Res. Commun.*, 2020, **526**, P. 206–212.
[60] Friebe B., Godenschweger F., Fatahi M., Speck O., Roggenbuck D., Reinhold D., Reddig A. The Potential Toxic Impact of Different Gadolinium-Based Contrast Agents Combined with 7-T MRI on Isolated Human Lymphocytes. *Eur. Radiol. Exp.*, 2018, **2**, 40.
[61] Lord M.S., Jung M., Teoh W.Y., Gunawan C., Vassie J.A., Amal R., Whitelock J.M. Cellular Uptake and Reactive Oxygen Species Modulation of Cerium Oxide Nanoparticles in Human Monocyte Cell Line U937. *Biomaterials*, 2012, **33**, P. 7915–7924.
[62] Ting S.R.S., Whitelock J.M., Tomic R., Gunawan C., Teoh W.Y., Amal R., Lord M.S. Cellular Uptake and Activity of Heparin Functionalised Cerium Oxide Nanoparticles in Monocytes. *Biomaterials*, 2013, **34**, P. 4377–4386.
[63] Asati A., Santra S., Kaittanis C., Perez J.M. Surface-Charge-Dependent Cell Localization and Cytotoxicity of Cerium Oxide Nanoparticles. *ACS Nano*, 2010, **4**, P. 5321–5331.
[64] Zamyatina E.A., Kottsov S.Yu., Anikina V.A., Popov A.L., Shevelyova M.P., Popova N.R. Cerium Oxide@silica Core-Shell Nanocomposite as Multimodal Platforms for Drug Release and Synergistic Anticancer Effects. *Nanosyst. Phys. Chem. Math.*, 2023, **14**, P. 560–570.
[65] Johnson K.K., Koshy P., Kopecky C., Devadason M., Biazik J., Zheng X., Jiang Y., Wang X., Liu Y., Holst J., et al. ROS-Mediated Anticancer Effects of EGFR-Targeted Nanoceria. *J. Biomed. Mater. Res. A*, 2024, **112**, P. 754–769.
[66] Zhou X., Wang B., Chen Y., Mao Z., Gao C. Uptake of Cerium Oxide Nanoparticles and Their Influences on Functions of A549 Cells. *J. Nanosci. Nanotechnol.*, 2013, **13**, P. 204–215.
[67] Mazzolini J., Weber R.J.M., Chen H.-S., Khan A., Guggenheim E., Shaw R.K., Chipman J.K., Viant M.R., Rappoport J.Z. Protein Corona Modulates Uptake and Toxicity of Nanoceria via Clathrin-Mediated Endocytosis. *Biol. Bull.*, 2016, **231**, P. 40–60.
[68] Butterfield A.D., Wang B., Wu P., Hardas S.S., Unrine J.M., Grulke E.A., Cai J., Klein J.B., Pierce W.M., Yokel R.A., et al. Plasma and Serum Proteins Bound to Nanoceria: Insights into Pathways by Which Nanoceria May Exert Its Beneficial and Deleterious Effects In Vivo. *J. Nanomedicine Nanotechnol.*, 2020, **11**, 546.

[69] Ryu N.-E., Lee S.-H., Park H. Spheroid Culture System Methods and Applications for Mesenchymal Stem Cells. *Cells*, 2019, **8**, 1620.
[70] Browning A.P., Sharp J.A., Murphy R.J., Gunasingh G., Lawson B., Burrage K., Haass N.K., Simpson M. Quantitative Analysis of Tumour Spheroid Structure. *eLife*, 2021, **10**, e73020.
[71] Pinto B., Henriques A.C., Silva P.M.A., Bousbaa H. Three-Dimensional Spheroids as In Vitro Preclinical Models for Cancer Research. *Pharmaceutics*, 2020, **12**, 1186.

Submitted 23 January 2024; revised 23 March 2024; accepted 26 April 2024

Information about the authors:

Danil D. Kolmanovich – Institute of Theoretical and Experimental Biophysics of the Russian Academy of Sciences, Pushchino, 142290, Russia; ORCID 0000-0003-3391-7889; kdd100996@mail.ru

Nikita N. Chukavin – Institute of Theoretical and Experimental Biophysics of the Russian Academy of Sciences, Pushchino, 142290, Russia; Scientific and Educational Center, State University of Education, Moscow 105005, Russia; ORCID 0000-0001-8431-4485; chukavinnik@gmail.com

Nikita A. Pivovarov – Institute of Theoretical and Experimental Biophysics of the Russian Academy of Sciences, Pushchino, 142290, Russia; ORCID 0009-0005-1997-0845; nikitapivovarov.workmail@gmail.com

Sergey A. Khaustov – Scientific and Educational Center, State University of Education, Moscow 105005, Russia; ORCID 0000-0001-9286-3644; sergeykhaustov@gmail.com

Vladimir K. Ivanov – Kurnakov Institute of General and Inorganic Chemistry of the Russian Academy of Sciences, Moscow, 119991, Russia; ORCID 0000-0003-2343-2140; van@igic.ras.ru

Anton L. Popov – Institute of Theoretical and Experimental Biophysics of the Russian Academy of Sciences, Pushchino, 142290, Russia; Scientific and Educational Center, State University of Education, Moscow 105005, Russia; ORCID 0000-0003-2643-4846; antonpopovleonid@gmail.com

Conflict of interest: the authors declare no conflict of interest.